Benchmark model of Quanser's 3 DOF Helicopter

Mirko Brentari, Paolo Bosetti, Isabelle Queinnec, Luca Zaccarian

Benchmark model of Quanser's 3 DOF Helicopter

Mirko Brentari, Paolo Bosetti, Isabelle Queinnec, and Luca Zaccarian

***Abstract*—This paper proposes a software benchmark tool for the Quanser *"3 DOF Helicopter"* in the *Mathworks Simscape* environment, based on a multi-body model of the experimental setup. The proposed benchmark tool takes into account a number of implementation features of the experimental setup and aims at providing a tool for simulative validation and performance analysis of control strategies. Along with this software-in-the-loop tool, a novel reduced complexity non-linear model for the Quanser *"3 DOF Helicopter"* is derived from the Lagrangian description of the full multi-body model, with the scope of being used in the control synthesis phase. The identification of the models parameters is carried out following a "gray-box" type of paradigm in order to match the models with the experimental setup. A feedback linearizing control law is as well proposed, based on the reduced complexity model. Closed-loop experimental results both show the accuracy of the simulated response compared to the experimental response, and the effectiveness of the proposed control strategy in a set-point regulation task.**

I. Introduction

Propeller-actuated aerial vehicles and UAVs are gaining increasing popularity (they are de-facto a standard) due to their simplicity and the availability of increasingly cheaper and lightweight control and sensing electronics. Nevertheless, due to their under-actuated nature, they represent an interesting and challenging control application. Many different architectures of propeller-actuated aerial vehicles have been proposed and studied, frequently in the VTOL (Vertical Take Off and Landing) configuration. Among these, consider the widespread quadrotors drones [1], ducted-fan configurations [2], and helicopter-like configurations [3].

The use of a benchmark platform both for research and educational purposes is a well established practice in these days. Quanser [4] is a Canada-based company that supplies a vast range of didactic platforms for control, robotics and mechatronics applications. Among these, a relevant propeller-based platform comprising many of the challenges of the VTOL configuration is the *"3 DOF Helicopter"*, because not only it is actuated by the nowadays vastly used propeller actuation, but it is underactuated and embeds a multi-body dynamics. It is composed by three rotational joints, with the end bar carrying a pair of propellers actuated by DC-motors. Measurements of the joints angles are supplied by incremental encoders and two power amplifiers are in charge of actuating the DC-motor/propeller assemblies. Both angular measurements and control voltages are then made available in *MATLAB-Simulink* environment.

For these reasons, Quanser's *"3 DOF Helicopter"* is considered a challenging application and a good benchmark example. Indeed, many works focusing on the control of this platform have appeared in the last years, proposing a variety of control strategies and focusing on different aspects. Among them, robust schemes are widely investigated. For example, [5] proposes two robust controllers based on sliding mode techniques, while [6] proposes a robust hierarchical controller. The authors of [7] focus on the regulation of two of the three helicopter's degrees of freedom thanks to a robust attitude control algorithm and an exogenous system in charge of generating the reference signals. Adaptive control seems to be another well investigated control strategy. Indeed, [8] makes use of the *"3 DOF Helicopter"* for experimentally validating an adaptive attitude controller based on the super-twisting algorithm, while in [9] the adaptive paradigm is addressed based on passivity and Implicit Reference Model techniques. In [10] an LMI procedure is proposed which allows designing simple adaptive control laws, while [11] focuses on an adaptive parameter identification algorithm. In [12], an adaptive controller is proposed which considers adaptation to parametric uncertainty, unmodeled dynamics, and actuator characteristics, while in [13] a nonlinear adaptive controller is considered, which includes a parameter identification scheme in the closed loop. In [14] a nonlinear model using a tree structure notation is developed, whose parameters are identified with an inverse dynamic model, while [15] deals with the trajectory tracking problem considering both state and input constraints in order to accomplish aggressive maneuvers. Finally, in [16] a nonlinear multivariable predictive controller is proposed, based on a each-sample-linearization of a neural network model of the nonlinear plant.

All of the above mentioned works are based on various reduced complexity models of the full helicopter dynamics. In this paper, instead, we propose the derivation of a full dynamical model of the Quanser *"3 DOF Helicopter"* experiment, based on a multi-body representation of the physical setup. Based on this representation, we develop a software-in-the-loop platform in the *MATLAB-Simulink* environment based on the *Simscape* package that takes into account a number of implementation features. We provide a downloadable version of this implementation as well, in order to make it usable by everyone for testing and validating control algorithms thereby obtaining reliable results before running actual experiments. We believe that this be a valuable benchmark, especially for teaching purposes but also for research results. Indeed, to the best of our knowledge, no reliable simulation model is available in the literature for this widespread experimental setup. In addition to the above, based on the Lagrangian representation of the full dynamical model, a reduced complexity model is also derived, with the scope of supplying a tool to be used in the control synthesis phase. Differently from past works, the reduced complexity model is derived with a

M. Brentari, P. Bosetti, and L. Zaccarian are with Dipartimento di Ingegneria Industriale, University of Trento, Italy.

L. Zaccarian and I. Queinnec are with LAAS-CNRS, Université de Toulouse, CNRS, France.

strong link to the full dynamical model in mind. Both the full model and the reduced one have been tuned in a system identification procedure using experimental data. A feedback-linearizing controller has been finally developed based on the reduced complexity model. This control strategy has been then tested on the simulation tools and on the real experiment, obtaining consistently desirable results.

The paper is organized as follows. In Section II a multi-body model of the Quanser *"3 DOF Helicopter"* is proposed. In Section III, the reduced complexity model is derived. The identification of the system parameters and the comparison of the proposed models with respect to the experimental setup is addressed in Section IV, while in Section V the synthesis of the control law is illustrated. Closed-loop experimental results and comparisons are reported in Section VI.

II. The Experimental Setup and Mechanical Model

The experimental setup considered in this work is the Quanser *"3 DOF Helicopter"* and we will refer to it as "the helicopter".

It is composed by a base on which an arm is connected by means of 2 revolute joints, one allowing the arm to rotate around the vertical axis (the "travel" motion), and one allowing the arm to tilt around the horizontal axis (the "elevation" motion). The helicopter body is mounted on one of the two extremities and it is allowed to tilt around the axis aligned with the arm (the "pitch" motion). It carries two propellers actuated by two DC-motors, which can generate a force that depends on the applied voltage. On the other arm extremity, a counterweight is mounted. The three "degrees of freedom" (*dof*), (i.e. the travel, the elevation and the pitch) are measured by three encoders with a resolution of 0.0015rad. A picture of the helicopter is reported in Figure 1.

Figure 1: Picture of the Quanser *"3 DOF Helicopter"*.

In order to study the helicopter motion, we now proceed with the illustration of a mechanical dynamical model (the "mechanical model" in the following) that fully describes the helicopter mechanical dynamics. This model is a lumped-mass model, with the mass concentrated in four points, two representing the counterweight and the arm, and the other two representing the two motor-propeller assemblies. In Figure 2, a representation of the model is depicted.

Some simplifying assumptions are exploited when deriving the mechanical model: the gyroscopic torques developed by the spinning motor-propeller assemblies are neglected, as well as the aerodynamic effects acting on the helicopter. The structure is considered as non deformable.

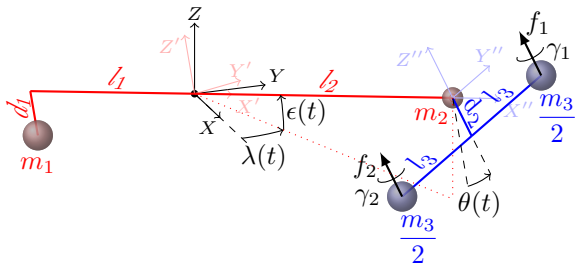

Figure 2: Mechanical model of the helicopter.

Let us start by defining an inertial Reference Frame (RF) $\{X\text{-}Y\text{-}Z\}$ whose origin corresponds to the point where the arm is connected to the base by means of the two revolute joints. We will refer to this reference frame as the "inertial RF". We consider the gravity acting along the negative Z direction with magnitude g. A second RF $\{X'\text{-}Y'\text{-}Z'\}$ (represented in light red in Figure 2) is obtained by applying to the inertial RF a Z-Y rotation sequence, corresponding respectively to a rotation of an angle $\lambda(t)$ (travel angle) and a subsequent rotation of an angle $-\epsilon(t)$ (elevation angle). The arm of the helicopter lays along the X'-axis: for this reason we call the $\{X'\text{-}Y'\text{-}Z'\}$ frame the "arm RF". The arm mass is concentrated at its extremities, therefore we place a first mass m_1 at $[-l_1, 0, -d_1]^\top$ and a second mass m_2 at $[l_2, 0, 0]^\top$, both in the arm RF. A third RF $\{X''\text{-}Y''\text{-}Z''\}$ (represented in light blue in Figure 2) is obtained starting from the arm RF and applying a translation of l_2 along the X'-axis and a rotation of an angle $\theta(t)$ (pitch angle) around the same axis. The helicopter body lays in this third RF, for this reason we refer to $\{X''\text{-}Y''\text{-}Z''\}$ as the "helicopter body RF". As mentioned before, the helicopter body mass m_3 is split in two halves, each one concentrated at one extremity of the helicopter body. Therefore, the two masses representing the motors-propellers assemblies are placed respectively at $[0, l_3, -d_2]^\top$ (front motor-propeller assembly) and at $[0, -l_3, -d_2]^\top$ (rear motor-propeller assembly), both coordinates being expressed in the helicopter body RF. Moreover, two lumped forces parallel to the Z''-axis are placed in correspondence to the two motor-propeller assemblies, respectively f_1 for the front and f_2 for the rear. These forces represent the forces generated by the spinning propellers. Finally, two torques γ_1 and γ_2 are applied at the same positions, representing the aerodynamics drag torques exerted by the propellers.

Without loss of generality, a constraint equation is added to the mechanical model, and it is such that the elevation equilibrium position corresponds to zero. This is done by selecting $m_1 = \frac{l_2}{l_1}(m_2 + m_3)$.

The friction at the joints has to be taken into account as well. While complex friction models, such as Coulomb friction, could be considered and implemented in the mechanical model, those highly nonlinear effect do not seem to be dominant in the experimental responses. Therefore, to reduce the model complexity we consider only linear viscous friction acting at each joint. Similar assumptions have been made in past works focusing on this experiment, for example in [9], [8], and in [10].

As the common practice, we assume that both the thrust forces f_1 and f_2 as well as the drag torques γ_1 and γ_2 exerted by the propeller have a quadratic relationship with the angular speed of the propellers themselves (see for example [17] and [18]). This leads to a linear relation between the thrust force and the drag torque (see for example [19]):

$$\gamma_i = k_{\gamma f} f_i \;\; i \in \{1, 2\}. \tag{1}$$

For the helicopter, the propellers are both right-handed, therefore $k_{\gamma f} < 0$.

The mechanical model introduced in this section fully describes the dynamics of the helicopter experiment, and can be used in order to validate a reduced complexity model that can be used for control design purposes. Moreover, it can be straightforwardly implemented in numerical physical simulation softwares such as *MathWorks Simscape* in order to simulate the helicopter dynamics and using it as a model-in-the-loop test platform for control strategies. Indeed, a *MathWorks Simscape* implementation of the proposed model is provided here (https://github.com/mrkrb/3dof_helicopter_benchmark), which embeds as well the identified parameters thanks to the procedure discussed further in the paper in Section IV.

III. Reduced complexity mathematical model

The aim of this section is to build a reduced complexity mathematical model of the helicopter that, in spite of its simplicity, captures the most relevant dynamic behavior of the real experiment. This model is useful in order to synthesize control laws, and we will refer to it as the "control model". The control model is constructed based on the mechanical model described in Section II, depicted in Figure 2.

The Lagrangian approach is widely used in order to compute the equations of motion of multi-body systems as the one of the helicopter (see, for example, [20, Chapter 7]).

The equations of motion of the system are obtained from the Lagrange equation:

$$\frac{\mathrm{d}}{\mathrm{d}t}\left(\frac{\partial \mathcal{L}}{\partial \dot{q}}\right) - \frac{\partial \mathcal{L}}{\partial q} = \xi \tag{2}$$

where $\mathcal{L} = \mathcal{K} - \mathcal{U}$ is the Lagrangian function defined as the difference between the kinetic $\mathcal{K}$ and potential $\mathcal{U}$ energies, $q \in \mathbb{R}^n$ is the vector of the generalized coordinates, and $\xi \in \mathbb{R}^n$ is the vector of the generalized forces associated to q. In the case of our mechanical model, we select $q(t) = [\lambda(t),\, \epsilon(t),\, \theta(t)]^\top$ (see Figure 2).

In general, for a mechanical system equation (2) can be written in the following standard form [20, Section 7.1.3]:

$$M(q)\ddot{q} + C(q, \dot{q})\dot{q} + R\dot{q} + g(q) = S(q)\tau \tag{3}$$

where $M(q)$ is a symmetric uniformly positive definite and uniformly bounded matrix representing the inertia of the system, $C(q, \dot{q})$ is a matrix associated to the Coriolis and centrifugal terms. R is a diagonal matrix of viscous friction coefficients, $g(q)$ represents the gravitational term, $S(q)$ is an $n \times m$ actuation matrix that maps the real input forces of the system $\tau \in \mathbb{R}^m$ into the generalized forces ξ.

In our case, we choose as τ as a combination of the input forces f_1 and f_2 exerted by the propellers (see Figure 2):

$$\tau := \begin{bmatrix} f_s \\ f_d \end{bmatrix} := \begin{bmatrix} f_1 + f_2 \\ f_1 - f_2 \end{bmatrix}. \tag{4a}$$

This choice allows us to obtain a more compact input matrix $S(q)$ and, as clarified in the following, it is more convenient during the control synthesis.

For the sake of conciseness, we report here only the terms R, $g(q)$, and $S(q)$, since the full $M(q)$ and $C(q, \dot{q})$ are very complex and not necessary for the derivation below:

$$R := \begin{bmatrix} r_\lambda & 0 & 0 \\ 0 & r_\epsilon & 0 \\ 0 & 0 & r_\theta \end{bmatrix}, \tag{4b}$$

$$g(q) := \begin{bmatrix} 0 \\ \dfrac{g}{l_1}\sin(\epsilon)(d_1 l_2 (m_2 + m_3) + d_2 l_1 m_3 \cos(\theta)) \\ g d_2 m_3 sin(\theta)\cos(\epsilon) \end{bmatrix}, \tag{4c}$$

$$\begin{aligned} S(q) := & \underbrace{\begin{bmatrix} -l_2\cos(\epsilon)\sin(\theta) & 0 \\ l_2\cos(\theta) & 0 \\ 0 & l_3 \end{bmatrix}}_{:=S_1(q)} + \\ & + \underbrace{\begin{bmatrix} k_{\gamma f}\cos(\epsilon)\cos(\theta) & l_3\sin(\epsilon) \\ k_{\gamma f}\sin(\theta) & 0 \\ 0 & 0 \end{bmatrix}}_{:=S_2(q)}, \end{aligned} \tag{4d}$$

where we emphasize the peculiar structure of the two terms S_1 and S_2 in the expression of $S(q) := S_1(q) + S_2(q)$ in (4d). This structure is motivated by the fact that we will consider $S_2(q)$ acting on the system as a bounded-time-varying disturbance, which will be neglected in the reduced complexity model. This results into having a decoupled input action on the λ-ϵ and on the θ dynamics.

The control model that we are going to introduce is a simplified version of the full equations of motion (3) of the mechanical model presented in Section II, where some terms are neglected after some assumptions. In particular, the following assumptions are made.

Assumption 1: The inertial coupling effects are neglected, and the diagonal part of $M(q)$ is constant or slowly varying. Moreover, the Coriolis and centrifugal term $C(q, \dot{q})\dot{q}$ is neglected.

We make this assumption because the terms $M(q)$ and $C(q, \dot{q})$ are the most convoluted ones and their contribution is not fundamental for reproducing the relevant part of the dynamical behavior of the helicopter, as confirmed later in the paper. Assumption 1 turns into having a diagonal and constant inertia matrix M and not having the $C(q, \dot{q})\dot{q}$ into the control model. Based on these assumptions, the following control model is obtained:

$$\ddot{q} = M^{-1}\left(-g(q) - R\dot{q} + S_1(q)\tau\right) \tag{4e}$$

where

$$M := \begin{bmatrix} j_\lambda & 0 & 0 \\ 0 & j_\epsilon & 0 \\ 0 & 0 & j_\theta \end{bmatrix}, \tag{4f}$$

j_i, $i \in q$ are constant parameters to be identified and

As one can notice, the control model (4) preserves the full gravitational term $g(q)$ and a part of the input matrix $S(q)$ of the mechanical model, at the cost of neglecting the complex terms of the inertial coupling between the different *dof*, the fictitious forces contained in the $C(q, \dot{q})$ term, and a part of the input matrix, which is considered to act on the system as a limited-time-varying disturbance. Even with these simplifications, in the following sections it will be shown that the relevant dynamical behavior of the helicopter is retained.

Model (4) will be tuned with a system identification procedure in order to reproduce as well as possible the helicopter dynamics.

Hereafter, we rearrange the equations of the control model (4) collecting the physical parameters into a set of non-redundant parameters to be identified.

$$\ddot{q} = -\overline{g}(q) - \overline{R}\dot{q} + \overline{S_1}(q)\tau \tag{5a}$$

where

$$\overline{g}(q) := M^{-1}g(q) = \begin{bmatrix} 0 \\ \sin(\epsilon)(a_{\epsilon 1} + a_{\epsilon 2}\cos(\theta)) \\ a_\theta \cos(\epsilon)\sin(\theta) \end{bmatrix}, \tag{5b}$$

$$\overline{R} := M^{-1}R = \begin{bmatrix} c_\lambda & 0 & 0 \\ 0 & c_\epsilon & 0 \\ 0 & 0 & c_\theta \end{bmatrix}, \tag{5c}$$

$$\begin{aligned} \overline{S_1}(q) :&= M^{-1}S_1(q) = \begin{bmatrix} -b_\lambda \cos(\epsilon)\sin(\theta) & 0 \\ b_\epsilon \cos(\theta) & 0 \\ 0 & b_\theta \end{bmatrix} = \\ &= \underbrace{\begin{bmatrix} -b_\lambda \cos(\epsilon) & 0 & 0 \\ 0 & b_\epsilon & 0 \\ 0 & 0 & b_\theta \end{bmatrix}}_{:=T(\epsilon)} \underbrace{\begin{bmatrix} \sin(\theta) & 0 \\ \cos(\theta) & 0 \\ 0 & 1 \end{bmatrix}}_{:=B(\theta)}. \end{aligned} \tag{5d}$$

The factorization of the input matrix $\overline{S_1}(q) = T(\epsilon)B(\theta)$ will be useful for the synthesis of the control law proposed in the following.

We thus obtain the following equations of motion:

$$\begin{aligned} \ddot{\lambda} &= -c_\lambda \dot{\lambda} - b_\lambda \cos(\epsilon)\sin(\theta) f_s \\ \ddot{\epsilon} &= -a_{\epsilon 1}\sin(\epsilon) - a_{\epsilon 2}\sin(\epsilon)\cos(\theta) - c_\epsilon \dot{\epsilon} + b_\epsilon \cos(\theta) f_s \\ \ddot{\theta} &= -a_\theta \cos(\epsilon)\sin(\theta) - c_\theta \dot{\theta} + b_\theta f_d \end{aligned} \tag{5e}$$

whose state is $q = [\lambda,\, \epsilon,\, \theta]^\top$ with $\dot{q}$, and whose input is $\tau = [f_s,\, f_d]^\top$. It is worth to point out that the factorization of the parameters of model (4) into the redundant parameters of (5) is not a reversible relationship, but it makes sense in a system identification procedure viewpoint as it will be commented in Section IV. Despite in literature many reduced complexity model of the experimental system of *Quanser* considered here [21] are present, the control model (5) is somewhat new and better justified than the existing ones in [6], [8], [9], [10], and [15], while preserving their core structure. In particular, in the reduced complexity model proposed in [6], the authors take into account a Coriolis contribution in the ϵ *dof*, while in [10] a variant of the input matrix is considered. In [8] and [15] slightly different input and gravitational effects are considered, while in [9] only the θ *dof* dynamics is taken into account, thanks to the same equation of motion considered in [10]. As a result, the reduced complexity models considered in these works are simpler than the one proposed here and there is no clear link between the multi-body dynamics and the reduced models.

Conversely, the control model (4) and (5) is preferable and more justifiable due to its clear and strong link with the Lagrangian representation of the equation of motion of the helicopter's mechanical model (3).

IV. Identification and responses comparison

In this section we describe the identification procedure followed in order to estimate the models parameters. A "gray-box model estimation" paradigm has been followed, in which the goal is the estimation of the model parameters of a known model. As outlined in Section II, in the experimental setup the input forces are generated by applying a voltage to each motor-propeller assembly. In the following subsection, the relation between the applied voltages and the exerted forces will be identified.

A. Input nonlinearity

Consider a τ in (4a) such that $f_d = 0$ and consider that the two motor-propeller assemblies are equal. Under these conditions, we can state that

$$f_s = h(v_s) \tag{6}$$

where $v_s = v_1 + v_2$ is the total voltage applied to the motors, and h is an unknown function that maps the total voltage v_s into the thrust f_s. Consider now the elevation dynamics in equation (5) at some equilibrium, with $\theta = 0$, and with a constant input $f_s = h(v_s)$:

$$-a_{\epsilon 1}\sin(\epsilon_{ss}) + b_\epsilon h(v_s) = 0 \tag{7}$$

By applying n different voltages $v_{s,k}$ $k \in \{1 \dots n\}$ spanning the allowed range $[-10,\, 10]$V ($[-5,\, 5]$V for each motor), it is possible to take n samples of a scaled version $\widetilde{h}$ of function h (and therefore a scaled version $\widetilde{f_s}$ of the thrust f_s) by observing the resulting steady state condition $\epsilon_{ss,k}$:

$$\widetilde{f_s} := \widetilde{h}(v_s) := c\, f_s = c\, h(v_s) = \sin(\epsilon_{ss}) \tag{8}$$

The voltage to be applied to a motor in order to exert a desired scaled force $\widetilde{f_i}$ can be then computed as:

$$v_i = \frac{1}{2}\widetilde{h}^{-1}(\widetilde{f_i}), \tag{9}$$

with $i \in \{1,\, 2\}$. Since we are identifying a scaled version of the thrust, we include as well a normalization procedure, such that the maximum applicable scaled force $\widetilde{f_i}$, $i \in \{1, 2\}$ corresponds to 1. Based on some experimental evidences and intuitions, $\widetilde{h}(v_s)$ has been selected to be a locally quadratic

and globally linear function based on the following piecewise description:

$$\widetilde{h}(v_s) := \begin{cases} p_2^- v_s + p_3^- & \text{if} \quad v_s \leq v_{sn} \\ p_1^- v_s^2 & \text{if} \quad v_{sn} \leq v_s \leq 0 \\ p_1^+ v_s^2 & \text{if} \quad 0 \leq v_s \leq v_{sp} \\ p_2^+ v_s + p_3^+ & \text{if} \quad v_{sp} \leq v_s \end{cases}, \tag{10}$$

where v_{sn} and v_{sp} represents threshold values specified below. This particular choice can be justified observing that the transfer function of a DC motor is such that in steady state conditions the rotational speed depends linearly on the applied voltage and on the applied load torque. Then for a DC motor with a propeller connected on its shaft, since both the thrust ad the aerodynamic load torque exerted by the propeller depend quadratically on the rotational speed, a linear relation between the voltage applied to the DC motor and the thrust exerted by the propeller is expected. Nevertheless, at slow rotational speed the aerodynamic load torque is negligible, and a quadratic dependence between the thrust and the voltage emerges.

A least square procedure has been then applied to identify the parameters of function (10), in order to best fit the experimental samples. C^1 continuity constraints of function (10) have been imposed during the optimization procedure. The threshold values v_{sn} and v_{sp} have been manually selected based on the measured points. The numerical values are reported in Table I. In Figure 3 both the experimental samples and the fitted function are depicted. Note that the function is non symmetric due to the propellers shape.

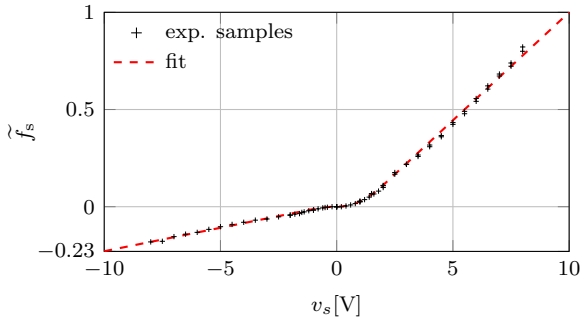

Figure 3: Input nonlinearity relation within the domain $[-10, 10]$V of the voltage input v_s.

Due to the fact that a scaled version of the forces $\widetilde{f}_s$ has been identified, we introduce the scaled input $\widetilde{\tau}$ acting on model (5) defined as:

$$\widetilde{\tau} = c\tau. \tag{11}$$

Due to this scaling, we will identify a scaled version of the input parameters of the control model b_λ, b_ϵ, b_θ, taking into account the scaling factor, i.e. $\widetilde{b}_\lambda = b_\lambda/c$, $\widetilde{b}_\epsilon = b_\epsilon/c$, $\widetilde{b}_\theta = b_\theta/c$.

B. Identification of the models parameters

Once the relation between the scaled version of the forces exerted by the two motor-propeller assemblies has been identified, the estimation of the model parameters can be faced. The identification procedure is based on a "gray-box" paradigm, both for the mechanical model and the control model, as detailed next.

parameter	c_λ	$\widetilde{b}_\lambda$	$a_{\epsilon 1}$	$a_{\epsilon 2}$	c_ϵ	$\widetilde{b}_\epsilon$
value	0.274	0.257	2.356	0.799	0.053	0.565
unit	$\frac{1}{\text{s}}$	$\frac{1}{\text{s}^2}$	$\frac{1}{\text{s}^2}$	$\frac{1}{\text{s}^2}$	$\frac{1}{\text{s}}$	$\frac{1}{\text{s}^2}$
parameter	a_θ	c_θ	$\widetilde{b}_\theta$	p_1^-	p_2^-	p_3^-
value	0.858	0.048	7.340	-0.012	0.024	0.012
unit	$\frac{1}{\text{s}^2}$	$\frac{1}{\text{s}}$	$\frac{1}{\text{s}^2}$	$\frac{1}{\text{V}^2}$	$\frac{1}{\text{V}}$	-
parameter	p_1^+	p_2^+	p_3^+	v_{sn}	v_{sp}	
value	0.028	0.111	-0.111	-1	2	
unit	$\frac{1}{\text{V}^2}$	$\frac{1}{\text{V}}$	-	V	V	

Table I: Control model identified parameters.

1) Identification of the control model: For the control model the "gray-box" identification has been carried out using *MATLAB* `idnlgrey` and `pem` tools, due to their suitability for identifying nonlinear systems. Firstly, the free motion of the ϵ-θ dynamics has been identified. This permits to have an estimate for the parameters of the autonomous part of the ϵ-θ dynamics in equation (5), i.e. $a_{\epsilon 1}$, $a_{\epsilon 2}$, c_ϵ, a_θ, c_θ. To this end, experiments with initial elevation and pitch angle different form zero and no voltages applied to the motors have been carried out. The parameters estimation resulting from this first identification procedure has then been used as a warm-start for the identification of the full motion. Forced experiments have been performed with input voltages consisting in a combination of steps in $\widetilde{f}_s$ and $\widetilde{f}_d$ applied to the helicopter. The resulting parameters estimation for the control model are reported in Table I.

2) Identification of the mechanical model: The identification of the mechanical model is more delicate than the one of the control model. First of all, there are more parameters to be identified. In addition to the lengths, masses and friction coefficients, there are the constant $k_{\gamma f}$ in equation (1) generating the aerodynamic drag torques, and the constant c in equation (11) needed to generate the real forces starting from the scaled forces. Secondly, the mechanical model is computationally heavier to be simulated. Moreover, there exist more than one realization of the mechanical model that produce the same responses of the experimental setup. Indeed, the same inertia properties can be achieved with infinitely many combinations of lengths and masses. For this reason, and in order to remove some degrees of freedom during the identification process, the length parameters l_1, l_2 and l_3 have been constrained to be similar to the ones of the real experiment. The experimental data used to tune the mechanical model are the same used to identify the control model. An initial manual tuning has been performed in order to fit as close as possible the free motion. Then, starting from this first tuning, an optimization procedure has been launched in order to refine the parameters with the aim of minimizing the RMS of the difference between the responses of the mechanical model with respect to the experimental responses. To this end, the *MATLAB* functions `lsqnonlin` and `ga` have been used, due to their flexibility

parameter	l_1	l_2	l_3	d_1	d_2	m_2
value	0.520	0.650	0.180	0.192	0.003	1.00
unit	m	m	m	m	m	kg
parameter	m_3	r_λ	r_ϵ	r_θ	$k_{\gamma f}$	c
value	0.771	0.250	0.050	0.003	-0.067	1.272
unit	kg	Nms	Nms	Nms	m	Nm

Table II: Mechanical model identified parameters.

and the good exploration properties of the genetic algorithm. The resulting parameters estimation for the mechanical model are reported in Table II.

Figure 4 shows the results of the identification procedure of both the mechanical model and the control model in the case of the experimental data used during the identification procedure (the identification set), while Figure 5 shows the responses in the case of experimental data different from the one used during the identification procedure (the validation set). Below each plot, a table reports the RMS of the difference between the experimental data and the models responses. From these tables it is possible to notice that in the case of the identification set, the mechanical model performs better than the control model, as expected. Except for the λ *dof*, this trend is present in the validation set as well. With regard to the λ *dof*, some observation can be done to justify the mismatch in the responses. Consider firstly the λ responses after 20s. Except for a rigid translation, here the trend of both the control model and the mechanical model are similar to the real one, with more detail fidelity produced by the mechanical model. The big difference is in the motion accumulated during the responses before 20s. This mismatch can be justified by considering that the λ dynamics is such that a non constant solution can only be experienced with a nonzero input. This makes the identification procedure of the λ *dof* harder and even a slight presence of dry friction can influence the response. Nevertheless, it will be shown that the closed-loop responses are such that this mismatch is compensated by the stabilizing controller.

V. Controller Design

The synthesis of a control law for the underactuated plant (5) is based on a time scale separation paradigm, where the travel λ and the elevation ϵ are treated as the slow dynamics, the pitch θ as faster than the latter two *dof*, and the neglected propeller dynamics between the commanded thrust (requested by the controller) and the exerted control input τ as the fastest quantity.

The controlled *dof* are the travel λ and the elevation ϵ, to which we will refer as $q_c := [\lambda, \epsilon]^\top$. The corresponding reference $q_{cr} := [\lambda_r, \epsilon_r]^\top$ is constant.

Firstly, we derive a feedback linearization control which relies on a virtual input $\nu \in \mathbb{R}^3$. Then, a reference value θ_r for the pitch angle and the input τ are selected in such a way to match the virtual input.

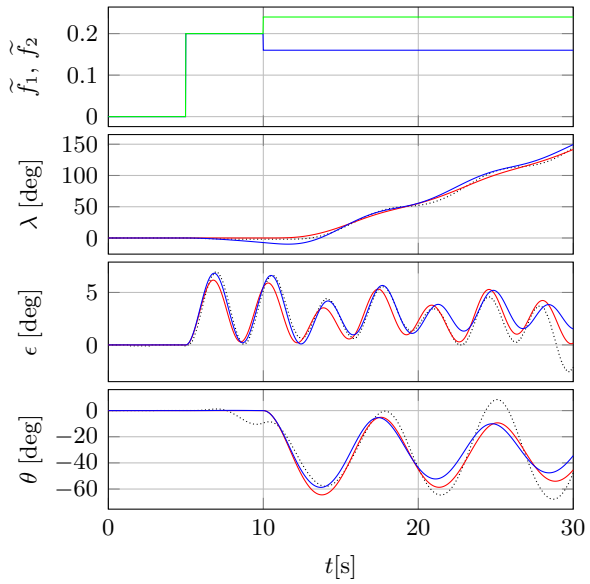

dof	RMS mechanical model	RMS control model
λ	2.805°	4.297°
ϵ	0.913°	1.070°
θ	6.835°	8.680°

Figure 4: Identification result of the mechanical and control model. Dotted: experiment. Blue: mechanical model. Red: control model. Blue: $\widetilde{f}_1$. Green: $\widetilde{f}_2$.

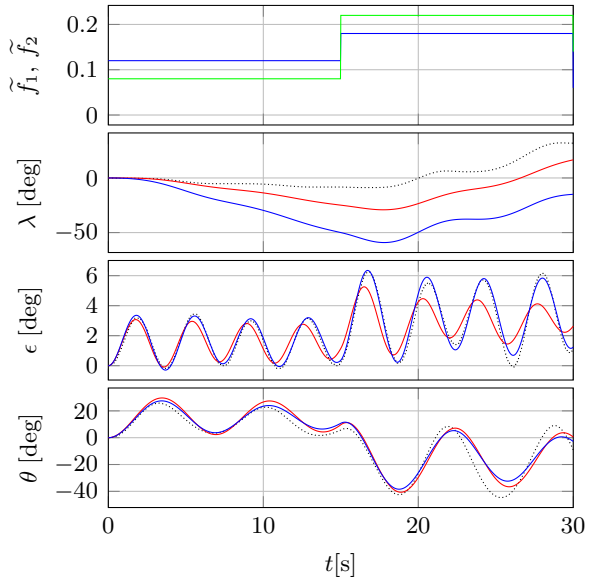

dof	RMS mechanical model	RMS control model
λ	36.723°	14.704°
ϵ	0.268°	0.897°
θ	5.749°	5.947°

Figure 5: Validation result of the mechanical and control model identification. Dotted: experiment. Blue: mechanical model. Red: control model. Blue: $\widetilde{f}_1$. Green: $\widetilde{f}_2$.

A. Feedback linearization

Considering q_{cr} as the constant reference for the controlled *dof* $q_c = [\lambda,\, \epsilon]^\top$, we define the tracking error as:

$$\widetilde{q} := \begin{bmatrix} q_c - q_{cr} \\ \theta - \theta_r \end{bmatrix} \tag{12}$$

Following a feedback linearization paradigm, we would like the dynamics of the mismatch $\widetilde{q}$ to behave like three decentralized damped oscillators, therefore we impose the following dynamics:

$$\dddot{\widetilde{q}} = \ddot{q} = -\Xi\ddot{\widetilde{q}} - \Omega^2\dot{\widetilde{q}} = -\Xi\dot{q} - \Omega^2\widetilde{q} \tag{13a}$$

where

$$\Omega := \mathrm{diag}(\omega_\lambda,\, \omega_\epsilon,\, \omega_\theta)\,, \tag{13b}$$

$$\Xi := 2\mathrm{diag}(\zeta_\lambda\omega_\lambda,\, \zeta_\epsilon\omega_\epsilon,\, \zeta_\theta\omega_\theta)\,, \tag{13c}$$

and $\zeta_i > 0$, $\omega_i > 0$, $i \in \{\lambda, \epsilon, \theta\}$ are tuning parameters and represent respectively the damping terms ζ_i and the natural frequency ω_i of the artificial damped oscillator dynamics. We now proceed in substituting equation (13a) into the underactuated plant dynamics (5a), which for the sake of clarity is here recalled

$$\ddot{q} + \overline{g}(q) + \overline{R}\dot{q} = T(\epsilon)B(\theta)\tau \tag{14}$$

Substituting equation (13a) in (14) it is possible to compute the virtual control action ν needed in place of $B(\theta)\tau$ in order to make the mismatch dynamics behave as specified in (13a):

$$\nu := T^{-1}(\epsilon)\left(\overline{g}(q) - \Omega^2\widetilde{q} - (\Xi - \overline{R})\dot{q}\right) + \nu_{\mathrm{ff}}\,, \tag{15}$$

noting that $T(\epsilon)$ defined in (5d) is diagonal and invertible thanks to the fact that $\cos(\epsilon) > 0$ due to the constraint on the elevation *dof* in the real experiment: $\epsilon \in [-15°,\ 15°]$. In (15) we introduced a feedforward term $\nu_{\mathrm{ff}} := [\nu_{\lambda\mathrm{ff}},\, 0,\, 0]^\top$ as a constant steady-state compensation acting on the first component of ν. This term improves the steady state tracking performance of the λ *dof* by compensating for the disturbance produced by the (1,1)-element of matrix $S_2(q)$ in equation (4d). Note that the $\cos(\epsilon)$ term present in the (1,1)-element of matrix $S_2(q)$ is matches with the same term in the matrix $T(\epsilon)$ that multiplies the virtual input ν.

With the above equation, we introduced the idea of using ν as a virtual input in order to make the underactuated system behave as a linear system. We now proceed in manipulating the virtual input in order to obtain the real input. We will compute an input τ and a reference value for the pitch dynamics θ_r in such a way that the real applied input produces an effect as close as possible to the desired one.

B. The virtual input

We would like $B(\theta)\tau$ to be as close as possible to the computed virtual input $\nu = [\nu_\lambda,\, \nu_\epsilon,\, \nu_\theta]^\top$ in equation (15). Considering the slow dynamics as constant, we define the mismatch between the desired virtual input and the applied virtual input:

$$\eta := \nu - B(\theta)\tau\,, \tag{16}$$

and the following objective function:

$$\begin{aligned} J(\theta,\tau) &:= \|\eta\|^2 = \|\nu - B(\theta)\tau\|^2 \\ &= \nu^\top\nu - 2\nu^\top B(\theta)\tau + \tau^\top\tau \end{aligned} \tag{17}$$

where we used that $B^\top(\theta)B(\theta) = I$. Consider therefore the following minimization problem:

$$\underset{\theta,\tau}{\mathrm{argmin}}\, J(\theta,\tau)\,. \tag{18}$$

The fact that the two optimization variables θ and τ belong to two different time scales suggests to solve the optimization problem (18) in two different steps: first, a desired value for the pitch (the slow quantity) is computed:

$$\theta^* := \underset{\theta}{\mathrm{argmin}}\, J(\theta,\tau) = \arctan\left(\frac{\nu_\lambda}{\nu_\epsilon}\right)\,, \tag{19}$$

then, the optimal value for τ for a general $\theta = \bar{\theta}$ is derived:

$$\begin{aligned} \tau^* := \underset{\tau}{\mathrm{argmin}}\, J(\bar{\theta},\tau) &= B^\top(\bar{\theta})\nu = \\ &= \begin{bmatrix} \nu_\lambda\sin(\bar{\theta}) + \nu_\epsilon\cos(\bar{\theta}) \\ \nu_\theta \end{bmatrix}. \end{aligned} \tag{20}$$

The resulting τ^* comes from basic computations, being $J(\theta,\tau)$ convex in τ. The result θ^* is as well simply derived and it is unique modulo 2π if $\tau_1 \neq 0$. Otherwise every value of θ zeroes out $J(\theta,\tau)$. We select the reference setpoint θ_r and the input τ as the optimal ones:

$$\theta_r = \theta^*\,,\ \ \tau = \tau^*\,. \tag{21}$$

As one can notice, θ^* (and thus θ_r) depends on ν_λ and ν_ϵ. Therefore, the control scheme can be applied as follows. Firstly, the first two component of (15) are computed in order to get ν_λ and ν_ϵ (note that (15) represents 3 independent equations). Secondly, θ_r is computed thanks to (19), which allows us to compute ν_θ with the third component of (15). Finally, τ is computed from (20).

C. State estimation

The feedback linearization control law proposed in equation (15) relies on the knowledge of both the *dof* position q and on the *dof* velocity $\dot{q}$. As discussed in Section II, the experimental setup is equipped with an encoder at each one of the three joints, which supplies a quantized measure with a resolution of 0.0015rad. Therefore only piecewise constant position measurements are available. In this paper, we follow an indirect approach where $\dot{q}$ has been estimated using the high-gain observation law proposed in [22] (see also [23] for the use of high-gain observers to estimate time derivatives). In particular, if we denote by x the collection of q and $\dot{q}$

$$x := [q,\, \dot{q}]^\top \in \mathbb{R}^6 \tag{22}$$

and if with $\widehat{x}$ we refer to the estimate of x

$$\widehat{x} := \left[\widehat{q},\, \widehat{\dot{q}}\right]^\top \in \mathbb{R}^6\,. \tag{23}$$

The estimator dynamics is given by

$$\dot{\widehat{x}} = \begin{bmatrix} 0 & I \\ 0 & 0 \end{bmatrix}\widehat{x} + \begin{bmatrix} k_p E^{-1} \\ k_v E^{-2} \end{bmatrix}(q - \widehat{q})\,, \tag{24}$$

parameter	ω_λ	ω_ϵ	ω_θ	ζ_λ	ζ_ϵ	ζ_θ
value	0.37	1.60	2.80	0.80	0.60	0.90
parameter	ε_λ	ε_ϵ	ε_θ	$\nu_{\lambda \text{ff}}$		
value	0.10	0.10	0.05	-0.08		

Table III: Controller and state estimator tuning.

where matrix $E \in \mathbb{R}^{3\times3}$ is a positive definite diagonal matrix containing the three decoupled high-gain scaling factors

$$E = \text{diag}(\varepsilon_\lambda, \varepsilon_\epsilon, \varepsilon_\theta)\,, \tag{25}$$

and $k_p\, k_v$ are two positive scalars such that the characteristic equation $s^2 + k_v s + k_p = 0$ has roots with negative real part. The three high-gain scaling factors ε_i, $i \in q$ are design parameters that can be conveniently adjusted in order to obtain a trade-off between smoothening action and reduction of the time lag of the estimator. Moreover, the smoothing action of the proposed approach mitigates the effect of the quantized position measurements. For these reasons, the control loop is in feedback from the estimated state $\hat{x}$.

VI. Closed-loop experiments and comparisons

In this section we discuss and compare the results obtained interconnecting a realization of the control scheme proposed in Section V to both the simulation platform and the experimental setup. Simulation results are obtained thanks to the mechanical model discussed in Section II.

A tuning process of the controller parameters has been carried out in order to obtain desirable evolutions. In particular, the natural frequencies in Ω have been chosen in such a way to respect the time scale separation discussed before, and in order to not reach the actuator limits in standard transient, while the damping parameters in Ξ have been chosen in such a way to obtain desirable transients with a slightly overshooting behavior. The presented results have been obtained using the same controller settings in both the experiment and the simulation. The used settings are reported in Table III.

The testing scenarios consist of a reference for the λ *dof* composed by a sequence of steps between $-90°$, $0°$, and $90°$, to be performed at a fixed constant reference for the ϵ *dof*. In particular, three experiments are presented, the first one with $\epsilon_r = 8°$, the second one with $\epsilon_r = 10°$, and the third one with $\epsilon_r = 13°$. The results are reported in Figure 6.

Let us start discussing the case with $\epsilon_r = 10°$, depicted in Figure 6b. First of all, it is possible to see that the simulation response matches well the experimental response, confirming that the proposed mechanical model is a good software-in-the-loop platform for testing and synthesizing control algorithm for the helicopter experiment. Observing the responses, we can claim that the proposed control algorithm succeeds in the stabilization and set-point regulation of the helicopter, producing a graceful evolution to the desired set-point. The step response of the λ *dof* exhibits the typical response of an over-critically damped oscillator, showing a non-overshooting behavior. A good tracking performance is present in the θ *dof* as well, while ϵ seems to be the most problematic *dof*. This is probably due to the disturbances produced by the term $S_2(q)$ in equation (4d), which has been neglected in the control model.

Moving to the experimental test with $\epsilon_r = 13°$, depicted in Figure 6c, similar considerations can be made. Observing the figure, it is possible to note that due to a larger value of ϵ_r in the fourth plot, the θ_r evolution in the fifth plots is in general smaller than in the two other cases. This is due to the fact that a larger ν_ϵ is needed to track a larger ϵ_r. This turns into having a smaller argument in the arctangent function in equation (19). Nevertheless, a larger ν_ϵ produces a larger $\widetilde{f}_s$, which amplifies the disturbance effect due to the neglected term $S_2(q)$ in equation (4d) (in particular due to the (1,2)-element). Indeed a larger tracking error of the ϵ *dof* is present in this case. Moreover, looking at the two upper plots it is possible to notice that a larger value of $\widetilde{f}_s$ turns into larger mean values of the two forces $\tilde{f}_1$ and $\tilde{f}_2$ than in the other cases, but the smaller θ_r in the fourth plot is such that smaller peaks are present.

The opposite trend holds in the case of the experiment with $\epsilon_r = 8°$ depicted in Figure 6a. Indeed, to track a smaller ϵ_r depicted in the fourth plot, a smaller ν_ϵ is needed, which turns into having a larger argument in the arctangent function in equation (19), which produces a larger θ_r in the last plot. Due to the fact that the θ controller is the most aggressive one, a larger θ_r produces larger peaks in $\tilde{f}_1$ and $\tilde{f}_2$ in the first two plots, which in the experimental setup lead to saturation.

VII. Conclusion and future works

In this paper, we firstly analyzed the multi-body dynamics of the Quanser *"3 DOF Helicopter"* and proposed a full dynamical model (the "mechanical model"), based on which we developed a software-in-the-loop testing platform. An implementation of the mechanical model in the *MATLAB-Simulink* environment is made available for free download and usage. This implementation has been proven to be a good software testing tool by means of experimental validation. Based on the Lagrangian representation of the mechanical model, a reduced complexity model has been derived (the "control model"). Both the mechanical and the control model have undergone a system identification procedure, in order to estimate the model parameters. The control model, despite its simplicity, captures the most relevant dynamical behavior of the helicopter as confirmed by the comparison with both the mechanical model and the experiment. This model then represents a good tool for control synthesis. Indeed, based on this reduced complexity model we developed a feedback linearizing control law, for which good set-point tracking performance has been validated both via simulation of the mechanical model and via experiments. Future work comprises the synthesis of saturation-aware control law based on anti-windup schemes, and the use of robust controllers including integral action to reject unknown biases.

Acknowledgement

The authors would like to acknowledge the valuable preliminary work of Vittorio Foroni during his MSc thesis at the LAAS-CNRS [24].

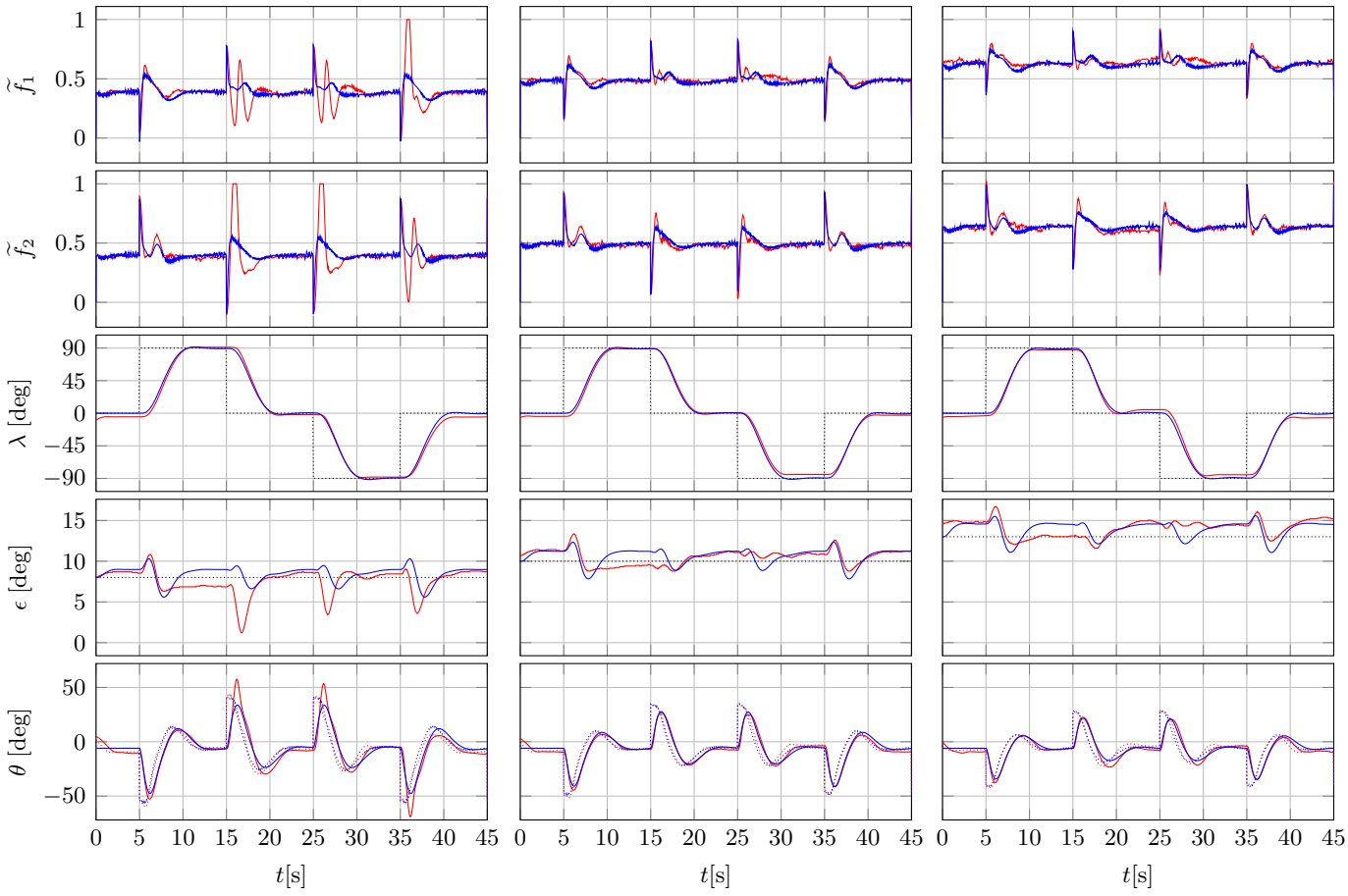

(a) Travel steps at $\epsilon_r = 8°$. (b) Travel steps at $\epsilon_r = 10°$. (c) Travel steps at $\epsilon_r = 13°$.

Figure 6: Experimental and simulation result in closed loop. Dotted curves: references. Blue curves: simulation with the mechanical model. Red curves: experiment.

REFERENCES

[1] M.-D. Hua, T. Hamel, P. Morin, and C. Samson, "Introduction to feedback control of underactuated vtolvehicles: A review of basic control design ideas and principles," *IEEE Control Systems*, vol. 33, no. 1, pp. 61–75, 2013.

[2] J. M. Pflimlin, P. Soueres, and T. Hamel, "Hovering flight stabilization in wind gusts for ducted fan uav," in *Decision and Control, 2004. CDC. 43rd IEEE Conference on*, vol. 4, pp. 3491–3496, IEEE, 2004.

[3] A. Isidori, L. Marconi, and A. Serrani, "Robust nonlinear motion control of a helicopter," *IEEE Transactions on automatic control*, vol. 48, no. 3, pp. 413–426, 2003.

[4] Quanser, "Quanser website." https://www.quanser.com/.

[5] H. Ríos, A. Rosales, A. Ferreira, and A. Dávilay, "Robust regulation for a 3-dof helicopter via sliding-modes control and observation techniques," in *American Control Conference (ACC), 2010*, pp. 4427–4432, IEEE, 2010.

[6] H. Liu, J. Xi, and Y. Zhong, "Robust hierarchical control of a laboratory helicopter," *Journal of The Franklin Institute*, vol. 351, no. 1, pp. 259–276, 2014.

[7] B. Zheng and Y. Zhong, "Robust attitude regulation of a 3-dof helicopter benchmark: theory and experiments," *IEEE Transactions on Industrial Electronics*, vol. 58, no. 2, pp. 660–670, 2011.

[8] A. Chriette, F. Plestan, H. Castañeda, M. Pal, M. Guillo, M. Odelga, S. Rajappa, and R. Chandra, "Adaptive robust attitude control for uavs–design and experimental validation," *International Journal of Adaptive Control and Signal Processing*, vol. 30, no. 8-10, pp. 1478–1493, 2016.

[9] A. L. Fradkov, B. Andrievsky, and D. Peaucelle, "Adaptive control design and experiments for laas "helicopter" benchmark," *European Journal of Control*, vol. 14, no. 4, pp. 329–339, 2008.

[10] D. Peaucelle, B. Andrievsky, V. Mahout, and A. Fradkov, "Robust simple adaptive control with relaxed passivity and pid control of a helicopter benchmark," *IFAC Proceedings Volumes*, vol. 44, no. 1, pp. 2315–2320, 2011.

[11] S. Le Gac, D. Peaucelle, and B. Andrievsky, "Adaptive parameter identification for simplified 3d-motion model of 'laas helicopter benchmark'1," *IFAC Proceedings Volumes*, vol. 40, no. 13, pp. 244–249, 2007.

[12] A. T. Kutay, A. J. Calise, M. Idan, and N. Hovakimyan, "Experimental results on adaptive output feedback control using a laboratory model helicopter," *IEEE Transactions on Control Systems Technology*, vol. 13, no. 2, pp. 196–202, 2005.

[13] M. Ishitobi, M. Nishi, and K. Nakasaki, "Nonlinear adaptive model following control for a 3-dof tandem-rotor model helicopter," *Control Engineering Practice*, vol. 18, no. 8, pp. 936–943, 2010.

[14] S. Rajappa, A. Chriette, R. Chandra, and W. Khalil, "Modelling and dynamic identification of 3 dof quanser helicopter," in *Advanced Robotics (ICAR), 2013 16th International Conference on*, pp. 1–6, IEEE, 2013.

[15] T. Kiefer, K. Graichen, and A. Kugi, "Trajectory tracking of a 3dof laboratory helicopter under input and state constraints," *IEEE Transactions on Control Systems Technology*, vol. 18, no. 4, pp. 944–952, 2010.

[16] J. Witt, S. Boonto, and H. Werner, "Approximate model predictive control of a 3-dof helicopter," in *Decision and Control, 2007 46th IEEE Conference on*, pp. 4501–4506, IEEE, 2007.

[17] P.-J. Bristeau, P. Martin, E. Salaün, and N. Petit, "The role of propeller aerodynamics in the model of a quadrotor uav," in *Control Conference (ECC), 2009 European*, pp. 683–688, IEEE, 2009.

[18] S. Formentin and M. Lovera, "Flatness-based control of a quadrotor helicopter via feedforward linearization," in *Decision and Control and European Control Conference (CDC-ECC), 2011 50th IEEE Conference on*, pp. 6171–6176, IEEE, 2011.

[19] R. Naldi, M. Furci, R. G. Sanfelice, and L. Marconi, "Global trajectory

tracking for underactuated vtol aerial vehicles using a cascade control paradigm," in *Decision and Control (CDC), 2013 IEEE 52nd Annual Conference on*, pp. 4212–4217, IEEE, 2013.
[20] B. Siciliano, L. Sciavicco, L. Villani, and G. Oriolo, "Robotics: modelling, planning and control, ser. advanced textbooks in control and signal processing," *Springer*, vol. 26, p. 29, 2009.
[21] Quanser, "3dof helicopter manual." Available at http://www.lehigh.edu/~inconsy/lab/frames/experiments/QUANSER-3DOFHelicopter_Reference_Manual.pdf.
[22] S. Nicosia, A. Tornambè, and P. Valigi, "Experimental results in state estimation of industrial robots," in *IEEE Conf. on Dec. and Contr.*, pp. 360–365, 1990.
[23] Y. Chitour, "Time-varying high-gain observers for numerical differentiation," *IEEE Transactions on Automatic Control*, vol. 47, no. 9, pp. 1565–1569, 2002.
[24] V. Foroni, "Nonlinear model identification and control design of a 3-dof laboratory helicopter," Master's thesis, University of Trento, March 2015.

Mirko Brentari received the M.Sc. degree (hons.) in Mechatronics Engineering in 2015 from the University of Trento (Italy). He is currently enrolled in the Ph.D. program in Mechatronics at the Department of Industrial Engineering of the University of Trento. In 2017-2018 he was a visiting scholar in the group of "Méthodes et Algorithmes de Commande" (MAC) at LAAS-CNRS, Toulouse (France). His research interests include hybrid and nonlinear control of aerospace vehicles and mechatronic systems.

Paolo Bosetti was born in Italy, on February 28, 1971. He received Ph.D. in Engineering of Materials and Structures from University of Trento, and he is currently Assistant Professor at the Department of Industrial Engineering at University of Trento. Main research focus is on intelligent manufacturing, following the paradigm of *sense, plan, control strategy* that is the reference of autonomous robots in other fields.

Isabelle Queinnec Isabelle Queinnec is currently CNRS researcher at LAAS-CNRS, Toulouse University. She received her PhD degree and HDR degree in automatic control in 1990 and 2000, respectively, from University Paul Sabatier, Toulouse. Her current research interests include constrained control and robust control of processes with limited information, with particular interest in applications on aeronautical systems, robotic, electronic, health, biochemical and environmental processes. She has been serving as member of the IFAC technical committees on "Biosystems and Bioprocesses" and on "Modelling and Control of Environmental Systems", respectively from 2002 and 2005 and of the IEEE CSS-CEB from 2013. She is currently AE for IET Control Theory and Applications and for the IFAC Journal NAHS (Nonlinear Analysis: Hybrid systems). She is co-author of a book on saturated systems and of more than 50 journal papers, both in control theory and in process engineering.

Luca Zaccarian (SM '09 F '16) received the Laurea and the Ph.D. degrees from the University of Roma Tor Vergata (Italy) where has been Assistant Professor in control engineering from 2000 to 2006 and then Associate Professor. Since 2011 he is Directeur de Recherche at the LAAS-CNRS, Toulouse (France) and since 2013 he holds a part-time associate professor position at the University of Trento, Italy. Luca Zaccarian's main research interests include nonlinear and hybrid control systems, modeling and control of mechatronic systems.